HHS Public Access

Author manuscript

Opt Lett. Author manuscript; available in PMC 2020 April 24.

Published in final edited form as:

Opt Lett. 2019 September 15; 44(18): 4546–4549. doi:10.1364/OL.44.004546.

Imaging Cherenkov photon emissions in radiotherapy with a Geiger-mode gated quanta image sensor

P Brůža[1], **A Pétusseau**[1,2], **S Tisa**[3], **M Jermyn**[4], **L A Jarvis**[5], **D J Gladstone**[1,5], **B W Pogue**[1,4]

[1]Thayer School of Engineering, Dartmouth College, 14 Engineering Dr, Hanover, NH 03755, USA

[2]Telecom Physique Strasbourg, University of Strasbourg, Pôle API, 67400 Illkirch-Graffenstaden, France

[3]Micro Photon Devices SRL, Via Stradivari 4, 39100 Bolzano, Italy

[4]DoseOptics LLC, 16 Cavendish Ct, Lebanon, NH 03766, USA

[5]Department of Medicine, Geisel School of Medicine, Hanover, NH 03755, USA

Abstract

Imaging of emitted single Cherenkov photons from human and animal tissue irradiated by X-ray and particle beams provides a unique way to monitor the accuracy of radiotherapy dose delivery in real time. However, achieving the necessary single-photon sensitivity in clinical room is challenging because of milliwatt level ambient room lighting and the presence of stray high-energy radiation. In this work, we demonstrate the first Cherenkov imaging with a time-gated quanta image sensor (QIS) employing a large single-photon avalanche diode (SPAD) array. Detecting single Cherenkov photons was possible owing to high photon avalanche gain, fast temporal gating, and moderately high ~7% quantum efficiency. Single-bit digitization and active SPAD quenching allowed stray X-ray noise suppression and enabled photon-noise limited imaging in clinical environment. This type of imaging allows knowledge of location, shape, and surface dose of the therapeutic beams radiotherapy with the stability of solid state detection.

Cherenkov radiation (CR) represents a visible broadband wavefront trailing behind a charged particle that propagates at superluminal velocity through matter [1]. The use of Cherenkov radiation as a diagnostic tool grew over decades from particle characterization experiments in high-energy physics and astrophysics through nuclear reactor fission rate measurements to single-cell molecular imaging [2–4] and external beam radiation therapy imaging applications [5–10]. Biomedical applications that employ the use of external beam of MeV X-rays or electrons benefit from direct dependency of CR on relative dose [5], and the fact that the CR is generated in the volume defined by the beam intersecting the tissue. In pre-clinical research, this Cherenkov excitation allows sub-millimeter 3D molecular imaging from whole body of small animals using concepts of light sheet microscopy [6, 7]. In clinical radiation oncology, near-infrared Cherenkov emission imaging of entrance and exit dose became a valuable tool for beam position and dose verification [8–10]. Imaging external beam excited CR in tissue requires single photon sensitivity in a photon-flooded scene of the operating room (Fig. 1a), since the clinical standards require that room lights must illuminate the patient to allow standard visual monitoring of the patient. Temporal gating synchronized with pulsed X-ray or electron delivery, as well as high intensifier gain

(10^6 typ.) are typical for clinical CR imaging. High imaging gain provides necessary single-photon sensitivity due to nanowatt/cm^2 fluence levels of CR, while the temporal gating allows background light suppression and luminescence lifetime imaging capabilities. Current imaging setups that rely on image intensifiers suffer from nonlinear response, long-term gain instability and sensitivity to overexposure. Importantly, the stray X-ray radiation impinging intensifier form a strong source of noise in the CR images, which limits the signal-to-noise and in turn the frame rate due to the necessity of temporal filtering. The value of SPAD-based sensors over intensifier-based imagers are 1) eliminated amplification-stage noise, 2) efficient X-ray noise rejection owing to binary photon registration, 3) capability of 10^3–10^5 frame-per-second readout rates, and 4) decreased complexity and size of the optoelectronic assembly. Therefore, the SPAD QIS shall provide superior performance for single-photon events in optically harsh environment, such as a radiation treatment room. Here we report, to the best of our knowledge, the first detection of weak Cherenkov emission from a water phantom and human tissue incited by clinical radiotherapy beams using a single-chip quanta imaging sensor. In addition, we compare the response of SPAD QIS and two types of modern image intensifiers to stray X-ray noise.

Cherenkov photons can be regarded as a surrogate to the radiation dose, deposited to the object by primary or secondary electrons whose kinetic energy is above the Cherenkov threshold (264 keV in water). To validate the linearity of SPAD detector response to Cherenkov photons, and therefore its linearity to projected dose distribution, we imaged the Cherenkov emission of water tank irradiated by 6 megavolt (MV) photon beams and 6 MeV electron beams of varying size (Fig. 2.a–d). The camera captured the images over 5 s, which corresponds to 0.5 Gy dose delivered to the volume in maximum dose region. The dose response linearity was verified by comparing the photon percent depth dose (PDD) profiles against a reference dosimetric dataset [15], as shown in top graph of Fig 2.e. The measured percent depth dose was averaged over 10 pixels in width and normalized to the maximum value. Both 6 and 10 MV PDD profiles showed a root mean square (RMS) error of 0.5%, confirming a very good intra-frame linearity of Cherenkov photon count to delivered dose.

Following the approved protocol from the Dartmouth College Investigational Review Board (IRB) for research involving human subjects, we were able to record the CR emitted from the patient during one fraction of breast cancer radiation therapy. Gating the SPAD synchronously with X-ray beam pulses was crucial for achieving acceptable level of Cherenkov signal to background noise. The camera's field of view covered an area of approximately 0.6×0.3 m^2. During the treatment we imaged two out of six beams, each delivering dose of 1.03 Gy and 1.33 Gy at maximum depth dose, respectively, to the extra-clavicular region of patient's body. A background image was captured prior the beam delivery in order to separate the CR from room-light image. During the beam delivery, each X-ray pulse of the linac incited Cherenkov emission, registered as 1–2 photons per pixel (ph·px^{-1}), on top of an approximately 1 ph·px^{-1} background. With 1.74 mm oversampled pixel resolution and 5 s exposure time, we achieved a signal to noise ratio (SNR) of 12 and 14 for the image of entrance and exit dose, respectively. Pixel dead time correction was not necessary, since the SPAD array operated in the linear range of the intensity response curve.

Quantitative single-photon counting renders the SPAD array a compelling quantitative optical detector of Cherenkov photon radiance, which can be used for in vivo imaging of absolute dose. Furthermore, the low dark current combined with fast temporal gating ensures that images are free of any background noise. It was shown [12] that the shape of observable Cherenkov emission is mainly governed by primary dose distribution, but the spectral radiance is highly affected by the Cherenkov photon transport through tissue. For absolute dose estimation, a careful calibration of the detective sensitivity and the optical parameters of the tissue are therefore vital. Attempts of measuring tissue optical properties and correcting the Cherenkov image were recently reported [12, 13]. We estimated the Cherenkov radiance L_{im} from the image using detective efficiency calibration. We scaled the detected photon counts-per-pixel I by per-pixel detective sensitivity ε:

$$L_{im} = \frac{I}{\varepsilon} = \frac{I}{\Omega A \eta_q} \quad 1)$$

which encompass the acceptance angle of the camera (Ω(f/1.4) = 1.00 ·10^{-4} sr), projected active area of one pixel (A = 3.02 mm^2), and average quantum efficiency of the photodiodes in the 600–900 nm wavelength range ($\eta_q \approx 0.07$, Fig. 1c). In the case of clinical imaging, the total detective sensitivity in the central image was therefore $\varepsilon = \Omega A \eta_q = 2.22 \cdot 10^{-5}$, which dropped to approx. 2.04 ·10^{-5} at the image edges due to lens vignetting. After a correction of the detective efficiency of the camera, we estimated the dose weighted radiance maps on the skin, shown in the Fig. 3.c and d. Maximum Cherenkov radiance values of 4.30×10^9 and 2.86×10^9 ph·sr^{-1}·cm^{-2}·s^{-1} were observed in the clavicular region the patient for the 10 MV exit and 6 MV entrance beams, respectively. These values correspond to an average radiant exitance of the Cherenkov light emitted from irradiated tissue of 3.4 and 2.6 nW/cm^2, assuming Lambertian emission profile of the skin.

SPAD array was expected to demonstrate high immunity against transient stray X-ray induced noise. Current Gen2+ and Gen3 intensifier-based imaging systems suffer from high sensitivity to high energy stray X-ray photons, which are detected as an impulse noise with power spectrum similar to the point spread function spectrum of the camera. GaAs photocathode-based intensifiers with improved PDE were found to be especially sensitive to hard radiation. Approaches like temporal median filtering [10] or various regularization methods [14] is typically used to minimize this effect. The SPAD array is expected to register these X-ray photon arrival events as single photon counts. To quantitatively compare the stray X-ray noise performance of SPAD QIS and both Gen2+ and Gen3 image intensifier based cameras, we recorded 100 darkfield frames gated to the X-ray pulse (360 Hz, 4 μs pulse width) accumulated over 18 linac pulses (equivalent to 20 fps) and under similar experimental conditions (3 m distance to linac isocenter). The SPAD image was oversampled similarly to the clinical setup. Static darkfield image stacks of 200 frames were recorded separately with artificial trigger signal, temporally averaged, and subtracted from the X-ray-gated darkfield frames. Resulting typical X-ray noise images (5×5 mm2) recorded by Gen2+ and Gen3-intensified CMOS cameras and SPAD QIS are shown in Fig. 4. The histogram of maximal intensities of each X-ray induced peak is plotted in Fig 4 as well. For clarity, both iCMOS image stacks were thresholded at two standard deviations (2σ) of the residual background noise prior peak detection, thereby excluding the very-low intensity

peaks which would be nearly indistinguishable from other noise sources (e.g. readout noise of iCMOS). The histogram reveals approximately an order of magnitude difference between the signal levels in Gen2+ and Gen3-based cameras. Most importantly, the SPAD QIS registered the X-ray events as single digital number counts. The observed level of noise in SPAD was lower than photon shot noise, typical for the clinical imaging setting. Comparing the noise power density for a given detection geometry, expressed as integral of digital counts per unit area and second, the SPAD outperforms Gen3 iCMOS by 3 orders of magnitude, and by a factor of 50 when compared to Gen2+ iCMOS.

In conclusion, we demonstrated for the first time a visualization and quantification of single Cherenkov photon events during clinical radiotherapy using a monolithic gated SPAD array. Furthermore, we have shown how a Geiger-mode operation of image detector pixels can effectively suppress a strong high-energy X-ray radiation background. The fast gating enabled us to image nanowatt-level, broadband Cherenkov radiation induced in the tissue of a radiotherapy patient, where room lights must be present and where spectral filtering is impractical. Major disadvantage of low fill factor of the SPAD active area and moderate spectral sensitivity in red spectral range is expected to be improved in near future with technological advances such as 3D chip stacking [18] and nanostructuring [19].

Methods

The Cherenkov radiation was induced by pulses of secondary high energy electrons during dose delivery to the target. The dose was delivered by collimated beam of polychromatic 6 and 10 megavolt (MV) X-ray photons produced as a 360 Hz pulse train of 4 μs X-ray pulses by a medical linear accelerator (linac; Varian Clinac, USA). In the water phantom imaging experiment, the beam was delivered to a body of water confined in a 40×35×35 cm3 clear acrylic tank. The camera was mounted at the base of the couch in distance of 2 m from beam isocenter, and used 135 mm f/2.0 collection lens. In the clinical imaging experiment (Fig. 1.d), the camera was set up to provide an approximate 1×1 m field of view of the radiotherapy patient using a 50 mm f/1.4 lens. The Cherenkov emission was expected to be detectable from areas where beam enters and exits patient's body, surface weighted to a depth of 3–5 mm (1/e value of surface emission) [8]. The SPAD camera was equipped with a 32×64 array [11] of Ø 30 μm SPAD pixels with 150 μm pitch (3.14% fill factor of SPAD active area), operated in Geiger counting mode with 60 ns dead-time. Each pixel included 8-bit photon counter (Fig. 1.a–b). Spectral sensitivity of the camera, plotted in Fig 1.c, matches the spectrum of Cherenkov emission in pure water. In clinical applications however, the hemoglobin and chromophores in tissue attenuate short wavelengths, which results in an average 7% photon detection efficiency of the SPAD. The camera was mounted at 3.2 m distance from target on a two-axis translation stage. The stage provided 30 μm sub-pixel-shift scanning in a 5×5 matrix parallel to the imaging plane, increasing the final image resolution to 160×320 pixels at the cost of 25× slower frame rate. Each SPAD counter was gated by a signal from X-ray target current probe ("TargI" signal) with duration of 4 μs. Using a 650 μs exposure time we captured a video stream of Cherenkov photon burst events at native 360 Hz frame rate. 73 frames were captured per each step during the pixel-shift scanning. The high-resolution image was therefore captured over a delivery of 0.5 Gy to the location of depth dose profile maxima. All images were corrected for dark current and flat-

field spatial distribution. In X-ray noise comparison experiment, we used optically coupled intensified CMOS cameras (DoseOptics LLC, USA) equipped with Ø18 mm red-sensitive Sb-K-Na-Cs Gen2+ and GaAs-O-Cs Gen3 intensifiers and the same 50 mm f/1.4 lens. The accompanying software was used to generate planned surface dose profiles, using the computer tomography (CT) image and treatment planning system (TPS, Varian Eclipse, USA) dose distribution.

References

1. Lamont MRE, Okawachi Y, and Gaeta AL Opt. Lett 38, 3478 (2013). [PubMed: 24104792]
2. Čerenkov PA, Phys. Rev 52, 378–379 (1937).
3. Robertson R, et al. Phys. Med. Biol 54, N355–N365 (2009) [PubMed: 19636082]
4. Thorek DL, et al. Am J Nucl. Med. Mol. Imaging 2(2), 163–173 (2012) [PubMed: 23133811]
5. Thorek DL, Ogirala A, Beattie BJ, and Grimm J Nat Med. 19(10), 1345–50 (2013) [PubMed: 24013701]
6. Glaser AK, et al. Med. Phys 40, 012101, 14 (2013) [PubMed: 23298103]
7. Pogue BW, et al. Nat. Bio. Eng 2, 254–264 (2018)
8. Bruza P, et al. Opt Lett. 41(13), 2986–9 (2016) [PubMed: 27367082]
9. Zhang R, et al. J. Biomed. Opt 18(11), (2013)
10. Jarvis LA, et al. Int. J. Radiat. Oncol. • Biol. • Phys 89(3), 615–622 (2014) [PubMed: 24685442]
11. Andreozzi JM, et al. Med Phys. 43(2), 993–1002 (2016) [PubMed: 26843259]
12. Bronzi D, et al. IEEE J. Select. Topics Quantum Electron 20(6), 354–363 (2014)
13. Zhang R, et al. J. Biophotonics 10(5), 645–656 (2017) [PubMed: 27507213]
14. Hachadorian R, et al. J. of Biomedical Optics 24(7), 071609 (2018).
15. Dong Y, et al. IEEE Trans. on Im. Proc 16(4), (2007)
16. Varian TrueBeam 10MV Eclipse data tables, Revision 1, Nov. 2012.
17. Ulku A, et al. IEEE Journal of Selected Topics in Quantum Electronics. PP(99) 1–1, (2018)
18. Charbon E Phil. Trans. R. Soc. A 372, 20130100 (2014). [PubMed: 24567470]
19. Zang K, et al. Nat. Comm 8 (628), 2017.

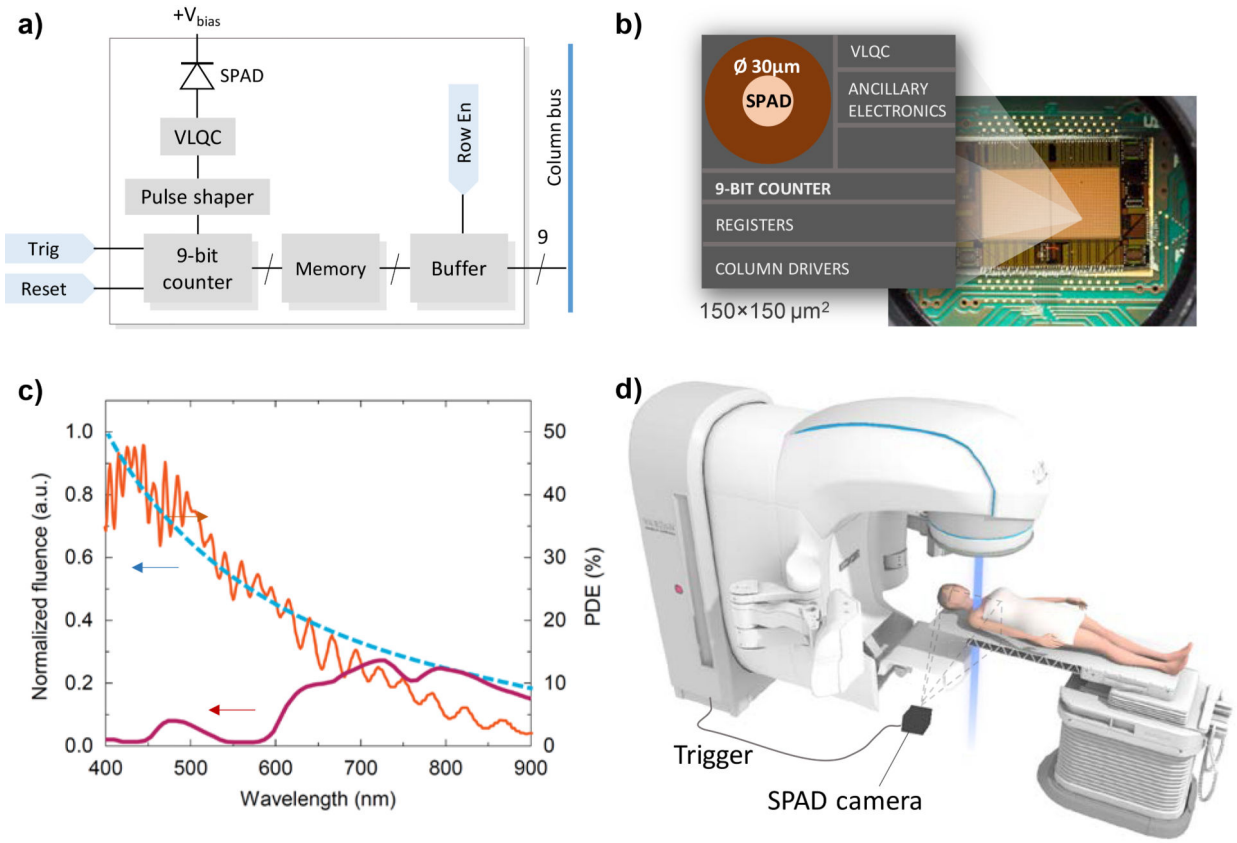

Fig. 1.

a) Simplified schematic diagram of a) single pixel circuitry and b) physical layout in SPAD Cherenkov detector (VLQC: variable load quenching circuit); c) Normalized Cherenkov emission in water (blue, dashed) and in tissue (purple), and the photon detection efficiency (PDE) of the SPAD detector (orange) [11]; d) Experimental set-up in the clinical radiotherapy suite.

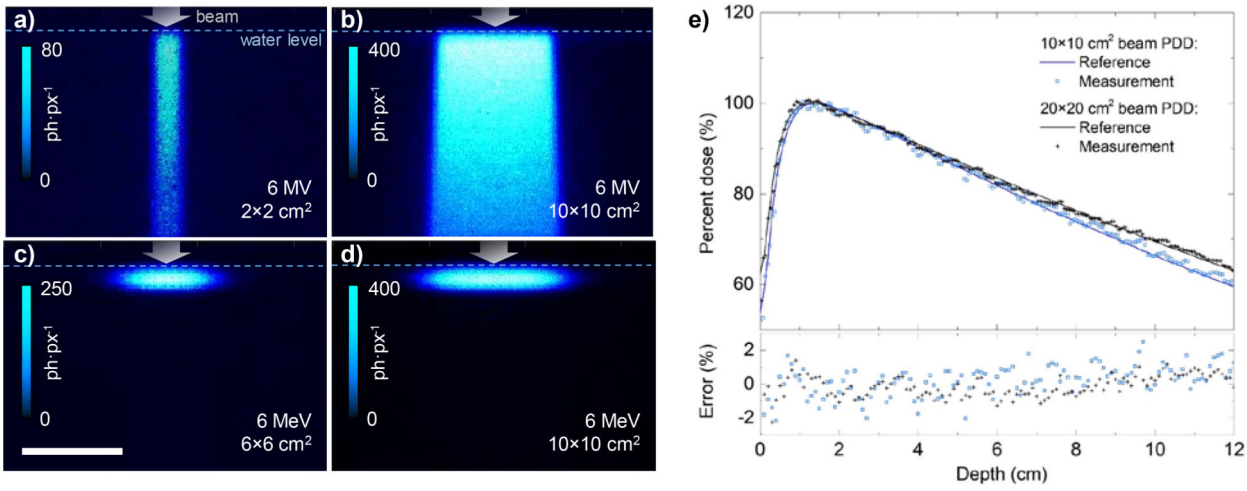

Fig. 2.

Cumulative Cherenkov emission resulting from delivery of 0.5 Gy dose to water phantom by 6 MV photon beam (a, b) and 6 MeV electron beam (c, d). Pixel size 1.7×1.7 mm^2 at object plane. e) Comparison of normalized Cherenkov emission profiles (“Measurement”) with reference dosimetric data [15] of a 10×10 and 20×20 cm^2 6 MV beam (top), and the resulting error (bottom).

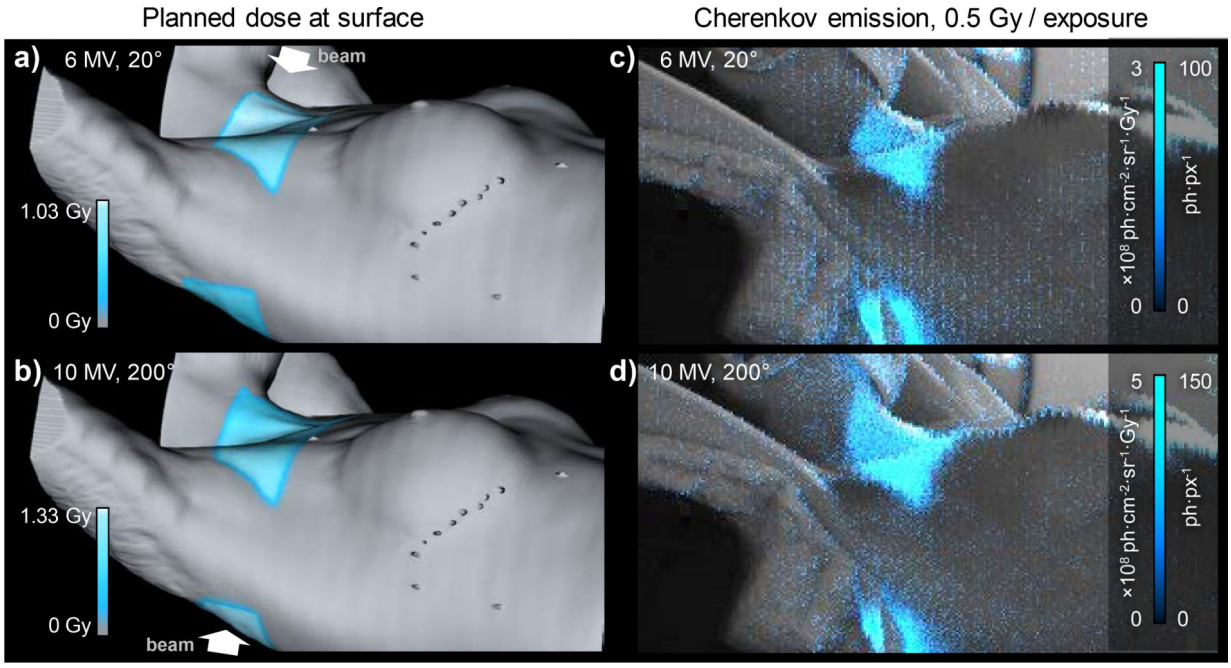

Fig. 3.

Planned surface dose profile (cyan) at the beam's entrance (a) and exit (b), calculated from patient's CT and TPS-based dose distribution. The surface dose corresponds an average dose value, exponentially weighted to 5 mm depth (1/e of max. intensity). c-d) Recorded Cherenkov emission (cyan) overlaid on a background image of the patient. The intensity scale reports measured photon counts ($ph \cdot px^{-1}$) and estimated radiance per unit dose ($ph \cdot cm^{-2} \cdot sr^{-1} \cdot Gy^{-1}$).

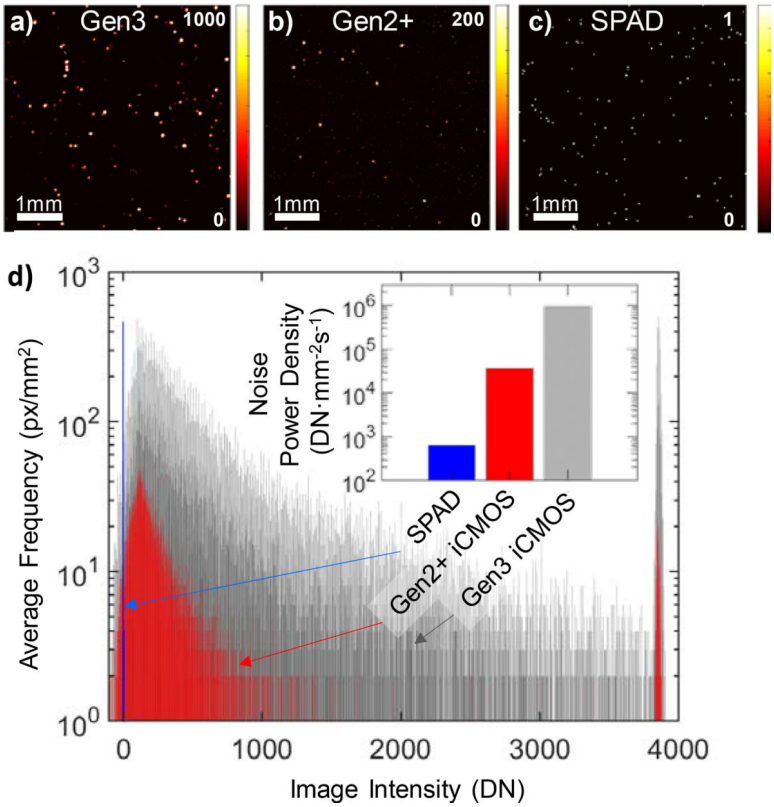

Fig. 4.

Response of single-photon sensitive cameras to stray X-ray noise. Top row: Typical response of a) Gen3 and b) Gen2+ intensified 12-bit CMOS detectors, and c) SPAD QIS accumulated over 18 linac pulses. d) Peak height distribution of X-ray induced impulse noise. Inset: Detected X-ray noise power density at distance 3 m from isocenter; signal intensity expressed in digital numbers.